

HUBBLE SPACE TELESCOPE SPACE TELESCOPE IMAGING SPECTROGRAPH OBSERVATIONS OF THE BIPOLAR JET FROM RW AURIGAE: TRACING OUTFLOW ASYMMETRIES CLOSE TO THE SOURCE¹

JENS WOITAS,² THOMAS P. RAY,³ FRANCESCA BACCIOTTI,⁴ CHRISTOPHER J. DAVIS,⁵ AND JOCHEN EISLÖFFEL²

Received 2002 April 18; accepted 2002 July 25

ABSTRACT

We have observed the bipolar jet from RW Aur A with STIS on board the *Hubble Space Telescope*. After continuum subtraction, morphological and kinematic properties of this outflow can be traced to within $0''.1$ from the source in forbidden emission lines. The jet appears well collimated, with typical FWHMs of 20–30 AU in the first $2''$ and, surprisingly, does not show a separate low-velocity component, in contrast to earlier observations. The systemic radial outflow velocity of the blueshifted lobe is typically 50% larger than that of the redshifted one with a velocity difference of about 65 km s^{-1} . Although such asymmetries have been seen before on larger scales, our high spatial resolution observations suggest that they are intrinsic to the “central engine” rather than effects of the star’s immediate environment. Temporal variations of the bipolar jet’s outflow velocities appear to occur on timescales of a few years. They have combined to produce a 55% increase in the velocity asymmetry between the two lobes over the past decade. In the red lobe, estimated mass flux (\dot{M}_j) and momentum flux (\dot{P}_j) values are around one-half and one-third of those for the blue lobe, respectively. The mass outflow to mass accretion rate is 0.05, the former being measured at a distance of $0''.35$ from the source.

Subject headings: ISM: Herbig-Haro objects — ISM: jets and outflows — stars: formation — stars: individual (RW Aurigae) — stars: pre-main-sequence

1. INTRODUCTION

Although there have been many studies of the propagation of outflows from young stars (see the reviews in *Protostars and Planets IV*), relatively little is known, from an observational perspective, about their generation (Eislöffel et al. 2000). A major problem is that the source itself is often embedded at optical/near-infrared wavelengths, making high-resolution observations, except in the radio band, impossible. That said, there are a number of optically visible young stars associated with outflows. Although their outflows are not as striking as those from more embedded young stars, such systems nevertheless represent the best window that we have on the “central engine.” With these ideas in mind, we have embarked on a *Hubble Space Telescope* (*HST*) program to examine outflows close to a small number of optically visible young stars (Bacciotti et al. 2000) including RW Aur, the subject of this paper.

RW Aur (HBC 80, HIP 23873) is a member of the Taurus-Auriga star-forming region. It is a binary system with RW Aur B located at a position angle of 258° and a projected separation of $1''.50$ with respect to RW Aur A (Leinert et al. 1993). Taurus-Auriga is usually assumed to have a distance of $\approx 140 \text{ pc}$ (Wichmann et al. 1998). In contrast, the *Hipparcos* distance of RW Aur is $70.5 \pm 34.0 \text{ pc}$, but as RW Aur is a close binary and variability shifts the system’s pho-

tocenter, the latter distance has been questioned (Bertout, Robinçon, & Arenou 1999). Here we will assume 140 pc, but one should keep in mind that this system may be closer. RW Aur A is one of the optically brightest T Tauri stars in the sky with $V = 10.1 \text{ mag}$ (Herbig & Bell 1988). The presence of strong $H\alpha$ emission [$\text{EW}(H\alpha) = 84 \text{ \AA}$; Herbig & Bell 1988] and high veiling at near-infrared wavelengths (Folha & Emerson 1999) categorize it as a classical T Tauri star (CTTS) with active accretion.

As is usual with CTTSs, accretion is accompanied by outflow. Hirth et al. (1994) first discovered an asymmetric bipolar jet (HH 229) from RW Aur A using long-slit spectroscopy and found that the blueshifted and redshifted jets on extended scales differed in absolute systemic velocity by a factor of 2. Another unusual property of this bipolar outflow is that the brighter lobe (in the red [S II] doublet) is redshifted. A detailed analysis of the spectroscopic data of Hirth et al. (1994) is presented in Bacciotti, Hirth, & Natta (1996), who showed that the redshifted jet from RW Aur A also has a low ionization fraction. Further observations by Mundt & Eislöffel (1998) of the area surrounding this star revealed that its flow is much more extensive than previously thought (with a total size of at least $145''$), while Dougados et al. (2000) examined the bipolar jet close to RW Aur A using adaptive optics.

Here we report on multiple observations with the Space Telescope Imaging Spectrograph (STIS) of the bipolar jet from RW Aur A that allow us to spatially resolve the jet not only along the outflow direction but transversely as well. This is the first bipolar YSO jet to be studied with STIS so close to its origin. Brief observational details are given in § 2, and our results are presented in § 3.

2. OBSERVATIONS AND DATA REDUCTION

The *HST*/STIS observations were made on 2000 December 10. Observing and data reduction procedures were

¹ Based on observations made with the NASA/ESA *Hubble Space Telescope*, obtained at the Space Telescope Science Institute, which is operated by the Association of Universities for Research in Astronomy, Inc., under NASA contract NAS5-26555.

² Thüringer Landessternwarte Tautenburg, Sternwarte 5, D-07778 Tautenburg, Germany.

³ School of Cosmic Physics, Dublin Institute for Advanced Studies, 5 Merrion Square, Dublin 2, Ireland.

⁴ I.N.A.F. Osservatorio Astrofisico di Arcetri, Largo E. Fermi 5, I-50125 Florence, Italy.

⁵ Joint Astronomy Centre, 660 North A’ohōkū Place, University Park, Hilo, HI 96720.

virtually identical to those employed for DG Tau (Bacciotti et al. 2000). Briefly, our seven STIS spectra of the RW Aur flow, taken with the G750M grating, included the brightest forbidden emission lines (FELs): [O I] $\lambda\lambda 6300, 6363$; [N II] $\lambda\lambda 6548, 6583$; [S II] $\lambda\lambda 6716, 6731$ along with H α . However, highly blueshifted ($v_{\text{hel}} \leq -235 \text{ km s}^{-1}$) [O I] $\lambda 6300$ emission was not recorded due to operating restrictions in the choice of STIS central wavelengths. The slit aperture was $52'' \times 0''.1$, while the spectral scale was $0.554 \text{ \AA pixel}^{-1}$. The nominal spatial sampling was $0''.05 \text{ pixel}^{-1}$, with an instrumental angular resolution of about $0''.1$ (FWHM) in the red. The slit was kept parallel to the blueshifted outflow axis (P.A. 130°) and offset to the southwest and northeast of the jet axis (corresponding to left and right, respectively, in the accompanying figures) in steps of $0''.07$ for a total coverage in the transverse direction to the jet of about $0''.5$. The slit was peaked on the source before offsetting. Since the position angle of the slit is roughly perpendicular to that of RW Aur B, the presence of this companion does not affect our observations.

We began our data reduction with pipeline spectra employing the most recent calibration files. After median filtering hot and dark pixels, the continuum contribution from RW Aur A (and its associated reflection nebula) was carefully removed. Very close to the star (i.e., less than $0''.1$), the continuum subtraction is critical. Despite this, the jet can be traced to at least $0''.1$ from RW Aur A in [O I] and [S II]. For smaller separations, there is no observed forbidden line emission above the continuum. This lack of emission is almost certainly caused by line-quenching effects close to the star, as in the case of DG Tau (Bacciotti et al. 2000).

Combining the spectra taken in the seven slit positions, we formed images of the flow (“channel maps”) in eight broad velocity bins for the lines mentioned above. The total velocity range covered is approximately -300 to $+300 \text{ km s}^{-1}$, which is split up into bins of $\Delta v \approx 75 \text{ km s}^{-1}$ (3 pixels). All velocities are quoted with respect to the mean heliocentric velocity of $+16 \text{ km s}^{-1}$ for RW Aur A reported by Petrov et al. (2001) and based on high-velocity resolution echelle data. In this paper, we present interesting and surprising results about the morphology and kinematics of the jet derived from the STIS spectra. The spatial distribution of physical parameters such as ionization, hydrogen density, or electron temperature, calculated from line ratios using a diagnostic code, will be the subject of another paper (F. Bacciotti et al. 2002, in preparation).

3. RESULTS AND DISCUSSION

As examples of the derived channel maps, we show [S II] $\lambda 6731$ (Fig. 1), [O I] $\lambda\lambda 6300, 6363$ (Fig. 2), and [N II] $\lambda 6583$ (Fig. 3). Figure 1 also contains estimates of the electron density N_e [cm^{-3}] derived from the line ratio of the red [S II] doublet (Osterbrock 1989). The morphology of the jet looks quite similar in the other lines except for H α , as discussed below. Our observations provide the first set of spectra of the RW Aur A jet with subarcsecond resolution. Compared to the previous study of Hirth et al. (1994), the spatial resolution is enhanced by an order of magnitude. Dougados et al. (2000) provided *images* of the jet at $0''.1$ angular resolution using adaptive optics and image deconvolution. They did not, however, detect jet emission closer than about $0''.4$ from the source. As we can trace the *redshifted* jet to within approximately 15 AU ($\approx 0''.1$) from the source in the FELs,

this is also an upper limit for the projected radius of any opaque disk around RW Aur A. By implication, such a disk is either seen almost edge-on or has a radius much less than 100 AU, i.e., the usually assumed size of a CTTS disk (Hartmann 1998). The latter could be the result of close encounters with RW Aur B, which, although currently separated from RW Aur A by at least 200 AU, may have an eccentric orbit. We estimate the jet inclination angle (i) with respect to the line of sight from a comparison of our channel maps with the images taken by Dougados et al. (2000) in 1997 December. If the jet knot at $d = 2''.8$ detected by Dougados et al. (2000) in [O I] and [S II] corresponds to the structure that we find at $d = 3''.4$ for intermediate velocities in the red lobe (marked with an A in Figs. 1 and 2), this indicates a tangential velocity $v_{\text{tan}} = 135 \text{ km s}^{-1}$. If we assume this is not a “pattern speed,” we can combine it with the radial velocity $v_r = 100 \text{ km s}^{-1}$ for the same knot derived from our spectrum to deduce $i = 53^\circ$. We do not attempt to measure proper motions for the knots closer to the source because the currently observed velocity differences between knots (see below) imply their morphology may have altered significantly (due to, e.g., knot merging) since the Dougados et al. (2000) observations. Given this, our value for i should be regarded as a rough estimate. In any event, even if the observed tangential velocity is a pattern speed, it is still a *lower* limit for the actual gas tangential speed (Eisloffel & Mundt 1998), and so it seems justified to assume $i \geq 53^\circ$.

A comparison of the forbidden line emission in the different lines shows that the [O I] emission appears stronger closer to the source than the [S II] emission. As pointed out by Shang et al. (2002), this is basically because hot, dense regions contribute more to the integral line-of-sight emissivity than cooler tenuous ones close to the star. In particular, although the electron density varies between 10^3 and $4 \times 10^3 \text{ cm}^{-3}$ along the jet beam, it increases dramatically close to the source. This makes the [O I] lines brighter than the [S II] lines at $|d| \leq 0''.5$, since the critical density for [O I] $\lambda\lambda 6300, 6363$ is 10^2 higher than that for the [S II] doublet. Contrary to the DG Tau case (Bacciotti et al. 2000), N_e is higher for moderate velocities in the red lobe. In the blue lobe, however, the highest density is found for the high-velocity bin. The jet is rather faint in [N II] emission (Fig. 3) in comparison to the other FELs and particularly with respect to [O I] $\lambda 6300$. This points toward a low ionization fraction in the observed portions of the jet, in agreement with results from previous diagnostic studies conducted at lower angular resolution (Bacciotti et al. 1996; Dougados, Cabrit, & Lavalley-Fouquet 2002). Also, the [N II]/[O I] and [S II]/[O I] ratios are similar in the red and blue lobes, which indicates similar ionization and excitation levels (Bacciotti & Eisloffel 1999).

Both the blue- and redshifted jets appear well collimated (Fig. 4, *top*). The convolved redshifted jet width (FWHM, measured in both [S II] $\lambda 6731$ and [O I] $\lambda 6300$ by binning together intermediate velocities) increases from $0''.1$ close to the source to $0''.2$ at $d \approx 2''$. In agreement with the determinations of Dougados et al. (2000), this suggests that the full redshifted jet opening angle (averaged over the corresponding projected distance) is less than 6° . Here we also show that similar behavior is observed for the blueshifted jet and that neither the red- or blueshifted jets are well resolved transversely at distances less than approximately 40 AU from RW Aur A. This implies a jet diameter in this region of less than 15 AU. For both the blue and red lobes, the values

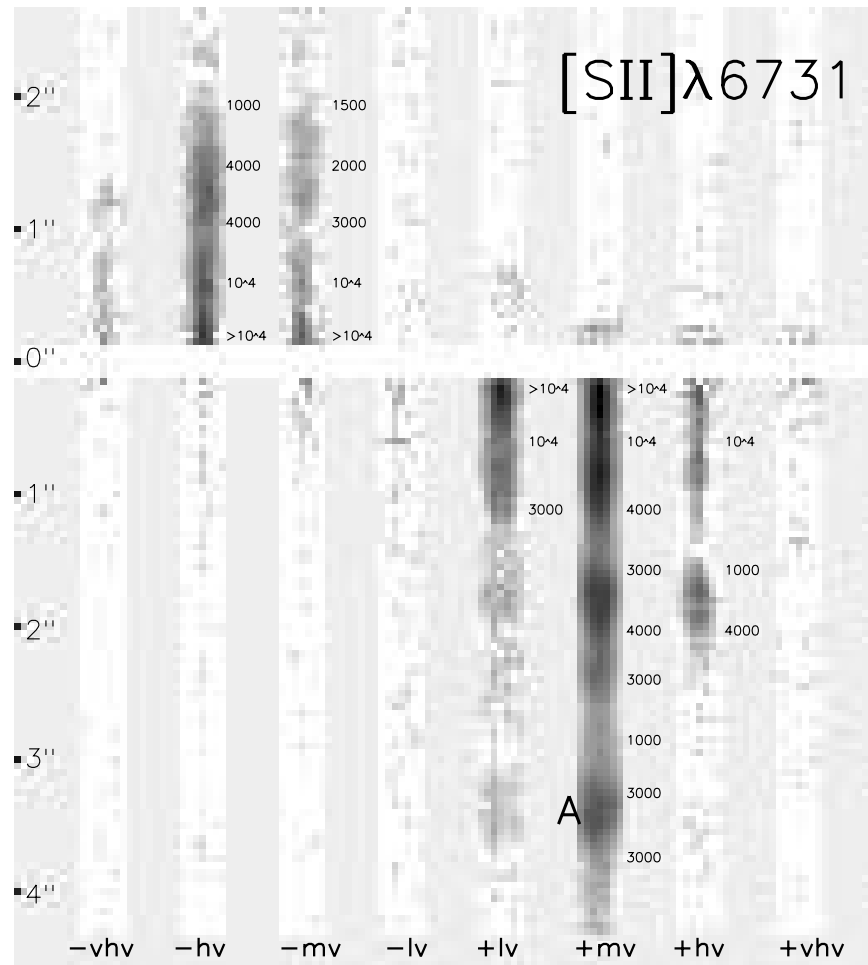


FIG. 1.—Images of the RW Aur jet in the [S II] $\lambda 6731$ line reconstructed from STIS spectra in different radial velocity intervals. These velocities are heliocentric and corrected for the heliocentric velocity of RW Aur ($+16 \text{ km s}^{-1}$, see text). Each panel has a width of $0''.5$. From left to right: -296 to -221 km s^{-1} ($-vhv$), -221 to -147 km s^{-1} ($-hv$), -147 to -73 km s^{-1} ($-mv$), -73 to $+1 \text{ km s}^{-1}$ ($-lv$), $+1$ to 75 km s^{-1} ($+lv$), 75 to 150 km s^{-1} ($+mv$), 150 to 224 km s^{-1} ($+hv$), 224 to 298 km s^{-1} ($+vhv$). The surface brightness is displayed logarithmically from 3×10^{-16} to $7 \times 10^{-13} \text{ ergs s}^{-1} \text{ arcsec}^{-2} \text{ cm}^{-2} \text{ \AA}^{-1}$. The numeric values are estimates of the electron density $N_e [\text{cm}^{-3}]$ derived from the ratio of the [S II] doublet.

plotted in Figure 4 are marginally consistent with those obtained from the X-wind model (see, e.g., Shang et al. 2002) and from self-similar magnetized disk wind models (Garcia et al. 2001), although for the latter, with only high accretion efficiencies. The corresponding low accretion efficiency disk wind model is expected to have even larger opening angles than observed (Garcia et al. 2001). Such a model might be appropriate for the DG Tau jet, whose jet width (FWHM) values, obtained from STIS data, are also shown for comparison in Figure 4 (top). The figure also suggests that the electron density is typically higher closer to the jet axis, as the FWHM widths measured in [O I] are almost everywhere smaller than the corresponding [S II] values. This statement is in agreement with most models of jet acceleration. Also, rather than having a constant opening angle, the jets from RW Aur A appear to expand more rapidly closer to the source (within $0''.5$) than farther away. Such behavior was, in fact, suggested by ground-based observations over a decade ago (Mundt, Ray, & Raga 1991) and seems to be supported by subsequent *HST* measurements (Hester, Stapelfeldt, & Scowen 1998; Reipurth et al. 2000). As pointed out by Reipurth & Bally (2001), for example, it is not clear how to interpret such results: the observed jet

widths may represent the extent of bow shock wings, and the true jets could be much narrower. We also note that farther than $0''.5$ from the source, there are indications for an anticorrelation between jet width and intensity, as already observed in *HST* images of the HH 34 jet (Ray et al. 1996).

In Figure 5, we present the [S II] $\lambda 6731$ line profiles at selected positions along the central slit for both the blue and red lobes. A Gaussian fit has been applied to find the center. Since the line profiles are, in fact, close to Gaussian and the residuals of the fit are only a few percent, the errors in the peak velocities will not be larger than 5 km s^{-1} . Over the whole range of separations covered by our observations, the velocity profiles of the lines only show one velocity peak at $v \approx 110 \text{ km s}^{-1}$ in the redshifted lobe or $v \approx -170 \text{ km s}^{-1}$ in the blueshifted lobe. In many CTTs, however, and in addition to this high-velocity component (HVC), the forbidden line emission has another component, the so-called low-velocity component (LVC) having typical radial velocities of -5 to -20 km s^{-1} (Hirth, Mundt, & Solf 1997) and a luminosity correlated with that of the HVC (Calvet 1997). Kwan & Tademaru (1988, 1995) have proposed that the LVC is the signature of a poorly collimated disk wind, while the HVC is a collimated jet close to the star. In the case of

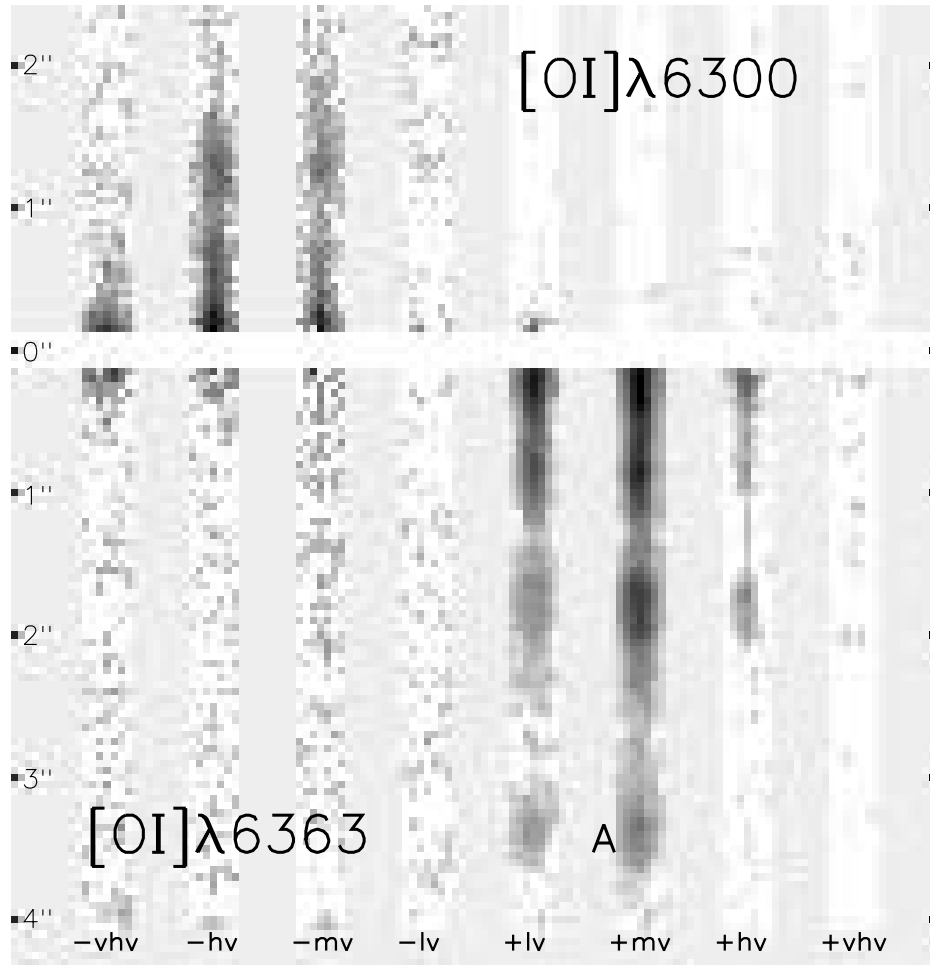


FIG. 2.—Same as Fig. 1, but for [O I] $\lambda 6300$ (redshifted lobe). For the blueshifted lobe, we use [O I] $\lambda 6363$ as a substitute since the velocity profile of [O I] $\lambda 6300$ is cut by the detector edge at $v_r = -235 \text{ km s}^{-1}$. From left to right: -318 to -240 km s^{-1} ($-vhv$), -240 to -162 km s^{-1} ($-hv$), -162 to -84 km s^{-1} ($-mv$), -84 to -5 km s^{-1} ($-lv$), 11 to 90 km s^{-1} ($+lv$), 90 to 169 km s^{-1} ($+mv$), 169 to 248 km s^{-1} ($+hv$), 248 to 328 km s^{-1} ($+vhv$). The surface brightness is displayed logarithmically from 10^{-15} to $1.5 \times 10^{-12} \text{ ergs s}^{-1} \text{ arcsec}^{-2} \text{ cm}^{-2} \text{ \AA}^{-1}$.

RW Aur, LVC emission was detected by Hartigan, Edwards, & Ghandour (1995) and Hirth et al. (1997) in the [O I] $\lambda 6300$ line. Based on observations performed in 1993 November, Hirth et al. (1997) measured an equivalent width ratio $\text{EW(LVC)}/\text{EW(HVC)} = 0.14$. This is approximately in line with the correlation found by Calvet (1997), according to which the LVC flux for the [O I] $\lambda 6300$ line should be $\approx 10\%$ of the observed HVC flux. Although such an LVC would be easily detectable in our STIS data, it is not present. To further illustrate this point, we have also spatially summed up our [O I] $\lambda 6300$ and [S II] $\lambda 6731$ line profile data $0''.5$ on either side of the peak stellar continuum position. The resultant line profiles are shown in the lower panel of Figure 5, where they are compared with the corresponding profiles obtained by Hartigan et al. (1995). The current lack of LVC emission is evident and indicates temporal variability on a timescale of a few years, as found by Solf (1997) for the DG Tau outflow. In the context of the Kwan & Tademaru model, this means that the RW Aur A disk wind (like the jet component) is variable, perhaps as a result of magnetic instabilities (Goodson, Böhm, & Winglee 1999). We also note that the absence of an LVC in RW Aur A is in line with recent [Fe II] $1.64 \mu\text{m}$ observations by C. J. Davis et al. (2002, in preparation). The lower panel of Figure 5 shows

that the LVC was not observed by either Hartigan et al. (1995) or ourselves in [S II] $\lambda 6731$. As the LVC often has a high electron density, this is not too surprising given the lower critical density of the [S II] $\lambda 6731$ line in comparison with the [O I] $\lambda 6300$ line.

In the top panel of Figure 5, the radial velocity of the blueshifted lobe of the RW Aur A jet is seen to exceed that of the redshifted lobe by a factor of 1.6 or $\approx 65 \text{ km s}^{-1}$. This has already been recognized by Hirth et al. (1994), but only for projected separations $\geq 300 \text{ AU}$ from RW Aur A. These authors also mentioned that radial velocity asymmetries in bipolar jets are not unusual and may be explained, for example, by different pressure gradients on both sides of the source. Using STIS, however, we have now shown that this behavior in the RW Aur A jet appears already at $d \approx 20 \text{ AU}$ from the star. Therefore, the origin of these velocity asymmetries must be located close to the “central engine” itself. Note also that asymmetries in the excitation and opening angle of the HH 30 bipolar jet were already evident on similar scales in WFPC2 data (Ray et al. 1996; Bacciotti, Eisloffel, & Ray 1999).

As can be seen in Figure 5, the radial outflow velocity varies between roughly 95 and 135 km s^{-1} in the red lobe and between -150 and -180 km s^{-1} in the blue lobe in the

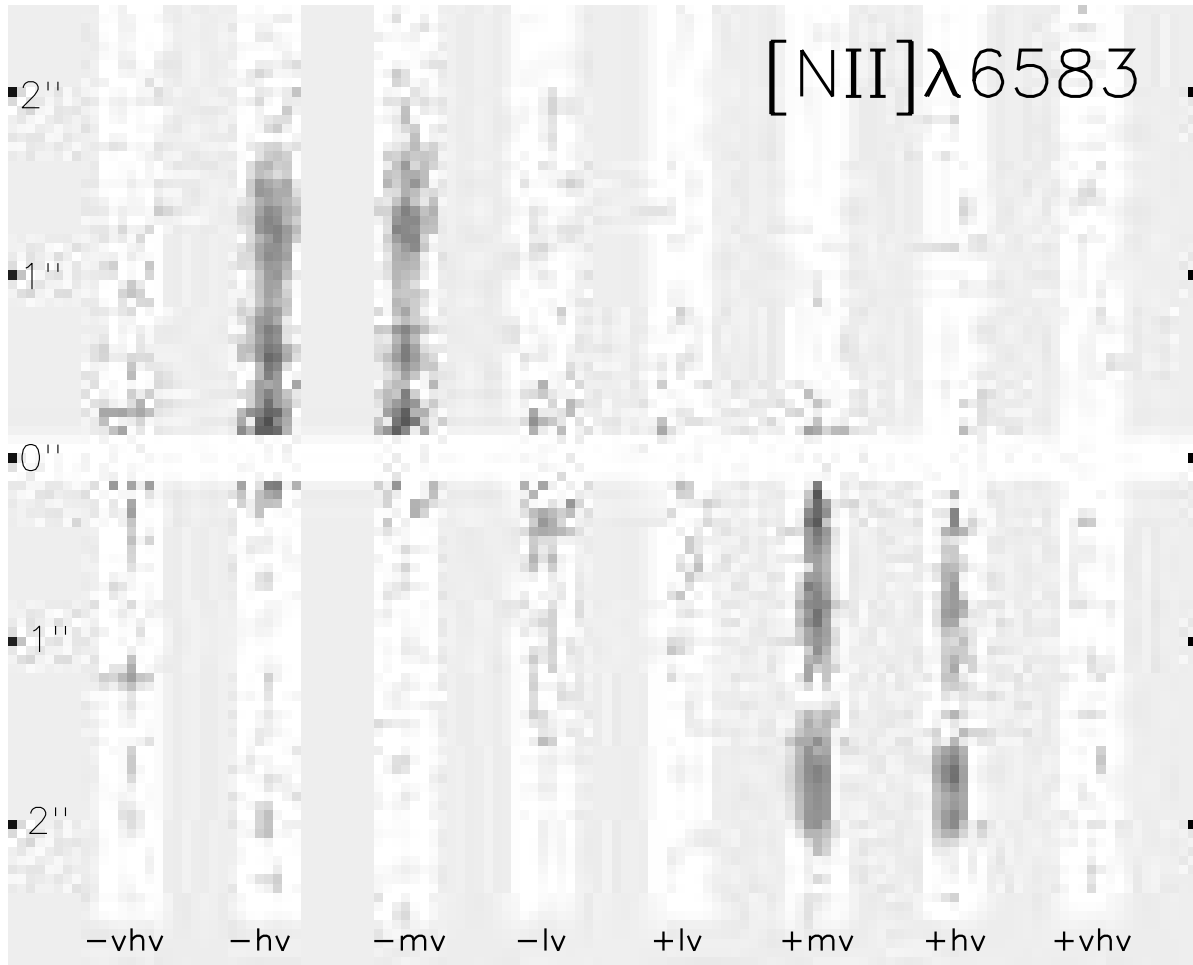


FIG. 3.—Same as Fig. 1, but for [N II] $\lambda 6583$. From left to right: -300 to -223 km s^{-1} ($-vhv$), -223 to -148 km s^{-1} ($-hv$), -148 to -72 km s^{-1} ($-mv$), -72 to $+4$ km s^{-1} ($-lv$), $+4$ to 79 km s^{-1} ($+lv$), 79 to 155 km s^{-1} ($+mv$), 155 to 230 km s^{-1} ($+hv$), 230 to 306 km s^{-1} ($+vhv$). The surface brightness is displayed logarithmically from 3×10^{-16} to 3×10^{-13} $\text{ergs s}^{-1} \text{arcsec}^{-2} \text{cm}^{-2} \text{\AA}^{-1}$.

separation range from $d = 0''.2$ to $d = 1''.7$. This could, in principle, be caused by the slit passing a “wiggling” jet, but there is no evidence of wiggling in our data. The position of the jet center, as derived from Gaussian fits to our velocity channel maps, changes along the jet by less than $0''.02$, which is much less than the slit width. In addition, these variations show no correlation with distance from the star, suggesting they are due to temporal variations in outflow velocity. As mentioned above, from a comparison of our channel maps with images of the RW Aur A jet from Dougados et al. (2000), we have estimated a jet knot proper motion of $\approx 0''.2 \text{ yr}^{-1}$. This implies that the observed velocity variations occur on a timescale of 1–3 yr. The knots of the RW Aur A jet may thus be “internal working surfaces” produced by variations in the outflow ejection properties as seen, for example, in the simulations of de Gouveia Dal Pino & Benz (1994).

The ratio $v_{\text{blue}}/v_{\text{red}}$ generally decreases from 1.75 at $d = 0''.2$ to 1.14 at $d = 1''.7$. Under the assumptions discussed above, this means that the velocity asymmetry increased by about 55% in the last decade. Such variations have not been reported in the past for any bipolar YSO jet and, as far as we are aware, this is the first time temporal evolution of bipolar jet asymmetry has been observed.

For both the red and the blue lobe, we have estimated the mass \dot{M}_j and momentum \dot{P}_j fluxes in the jet at the distances from the source quoted in Figure 5. Toward this aim, we used our determinations of velocity, inclination angle, electron density, and jet width (FWHM), combining them with the estimates of the hydrogen ionization fraction in Dougados, Cabrit, & Lavalley-Fouquet (2002). The latter is reported to vary between 0.007 and 0.09 between $0''.4$ and $1''.7$ in the redshifted jet, and we have assumed that the ionization fraction in the blue lobe has the same values. As already mentioned, this statement is supported by the similarity of the [N II]/[O I] ratio observed along the two lobes. We take as the dynamical diameter of the jet the measured FWHM and a constant space velocity over the jet transverse section. The first assumption may lead to underestimating the fluxes if the peripheral regions of the flow are too cold to be observable, but the second hypothesis should counterbalance the effect since, according to theoretical models, the colder external regions are moving more slowly. Our results are summarized in the bottom panels of Figure 4. We find that in the blue lobe, \dot{M}_j varies from ~ 1.1 to $10^{-7} M_{\odot} \text{ yr}^{-1}$ at $0''.35$ from the source to $\sim 1.2 \cdot 10^{-8} M_{\odot} \text{ yr}^{-1}$ at $1''.5$, while within the same range, \dot{P}_j varies from $\sim 3.8 \times 10^{-5}$ to $\sim 3.5 \times 10^{-6} M_{\odot} \text{ yr}^{-1} \text{ km s}^{-1}$. In the red lobe, the values for \dot{M}_j and \dot{P}_j are typically one-half and one-third, respectively,

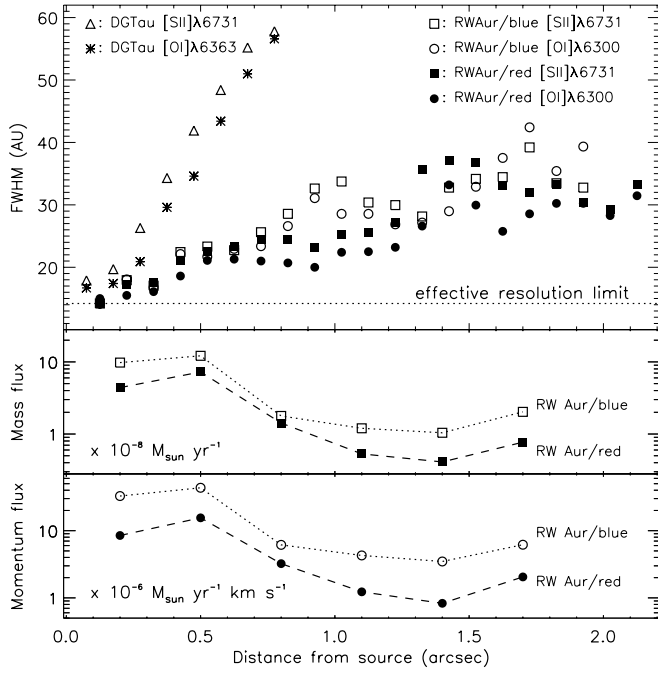


FIG. 4.—*Top*: Plot of FWHM width vs. angular distance from the source for the blue- and redshifted jets from RW Aur A in [O I] $\lambda 6300$ and [S II] $\lambda 6731$. All widths are measured binning together intermediate velocities. For comparison, we also show the blueshifted jet from DG Tau, which is seen to have a much wider opening angle. The effective resolution limit is the empirical FWHM of a reconstructed image of the source. *Bottom panels*: Mass flux (per $10^{-8} M_{\odot} \text{ yr}^{-1}$) and momentum flux (per $10^{-6} M_{\odot} \text{ yr}^{-1} \text{ km s}^{-1}$) at selected positions along the blue and red lobes of the RW Aur jet.

of those in the blue lobe. In both lobes, the fluxes are seen to decrease by about an order of magnitude in less than $2''$ from the source. If the knots represent mini working surfaces, this finding might be justified by the fact that a considerable fraction of the jet material is pushed sideways. Alternatively, the calculation might be affected by the fact that the jet is less and less excited moving away from the source, and the measured FWHM becomes indeed substantially smaller than the jet dynamical diameter. The mass accretion flux for this star is $1.6 \times 10^{-6} M_{\odot} \text{ yr}^{-1}$ (Hartigan, Edwards, & Ghandour 1995); thus, averaging over the two lobes, one finds $\dot{M}_j/M_{\text{acc}} \sim 0.05$ close to the source, which is in line with theoretical predictions of jet-launching models. Although the origin of the blue/red asymmetries remains unknown, one might ask if the observed imbalance between the momentum fluxes in the two lobes may cause dynamical effects on the overall system. We have calculated that if such imbalance persisted for all the pre-main-sequence lifetime of this star, it should have caused a recoil (space) velocity of 8 km s^{-1} or less for the system. This value, on the other hand, is probably itself a gross overestimate because (1) RW Aur has already accreted most of its mass, and it may have acquired this material in a more symmetrical way, or (2) over time, linear momentum balance may be maintained.

As a final remark, we mention that in $H\alpha$, the appearance of the region close to the source largely differs from the FELs. The $H\alpha$ emission can be traced back to the stellar position in both lobes, and there are two $H\alpha$ velocity peaks

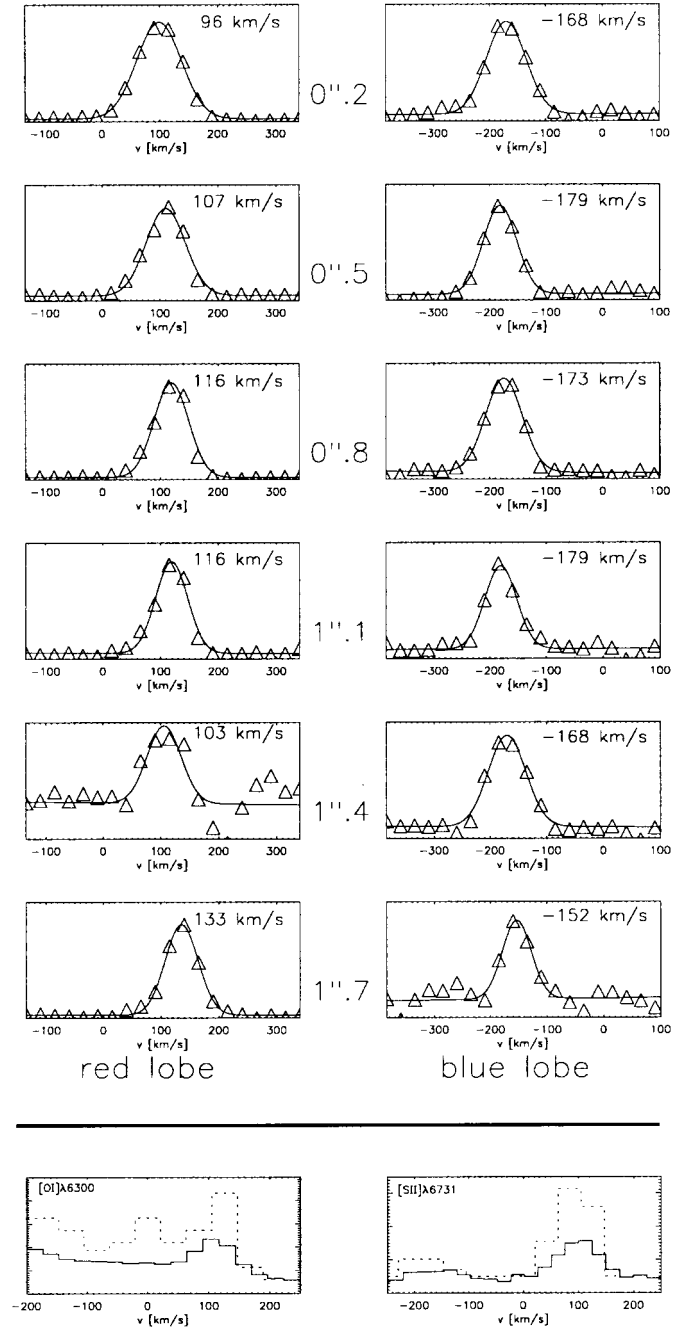


FIG. 5.—*Top*: Gaussian fits to the velocity profile of the red and blue lobes for the [S II] $\lambda 6731$ line as derived from the central slit position and for different projected separations from the source. Numbers inside the panels are systemic peak velocities with uncertainties of less than 5 km s^{-1} . *Bottom*: Comparison of the [O I] $\lambda 6300$ and [S II] $\lambda 6731$ line profiles from Hartigan et al. (1995; dashed lines) with the spatially averaged STIS equivalents (solid lines). For details see text.

on the star with the same velocities as the blue- and redshifted lobes of the jet, suggesting that we are tracing them back to their source. It has been claimed (see, for example, Hartmann 1998) that $H\alpha$ emission is a tracer not only of outflow but of inflow as well. In particular, accreted material, channelled into funnel flows by the stellar magnetic field, may contribute to the $H\alpha$ line profile. We do not see any evidence for such a contribution here.

4. CONCLUSIONS

We have obtained spectra of the bipolar jet of RW Aur A at an unprecedented high spatial resolution of $0''.1$, and for the first time, studied its morphological and kinematic properties within $1''$ from its origin. Both outflow lobes can be traced as close as $0''.1$ from the source in the FELs. In $H\alpha$, the STIS spectra show two strong maxima on the star, with radial velocities coinciding with those of the two outflow lobes. The jet appears well collimated very close to its origin and asymmetries in the red- and blueshifted lobe velocities arise within a region smaller than 20 AU from the source. This scale is almost certainly a conservative estimate, as our values for the jet inclination angle to the line of sight and distance to RW Aur are lower and upper limits, respectively.

In contrast to previous observations, we do not find a separate low-velocity outflow component, which indicates this feature is variable on timescales of a few years. If this component is a disk wind, then our observations imply such winds vary on similar timescales as the higher velocity out-

flow and may also be episodic. Variations in the high-velocity components in the RW Aur A jet suggest that its knots may be internal working surfaces. This is also supported by our estimates of the mass and momentum fluxes, which in both lobes are observed to decrease by at least an order of magnitude within the first $2''$ from the source. Close to the star, we find an average mass flux of about $8.5 \times 10^{-8} M_{\odot} \text{ yr}^{-1}$, which is about 5% of the mass accretion flux. The mass flux and momentum flux values in the red lobe are typically one-half and one-third of the values in the blue lobe, respectively. Finally, we note that velocity variations in the blue- and redshifted lobes imply an increase in the radial velocity asymmetry of about 55% over the last decade.

J. E. and J. W. acknowledge support by the Deutsches Zentrum für Luft- und Raumfahrt (grant 50 OR 0009). T. P. R. also wishes to thank Enterprise Ireland for support (grant SC/2000/252). The authors appreciate useful discussions with Reinhard Mundt and the very helpful comments of an anonymous referee.

REFERENCES

- Bacciotti, F., & Eislöffel, J. 1999, *A&A*, 342, 717
 Bacciotti, F., Eislöffel, J., & Ray, T. P. 1999, *A&A*, 350, 917
 Bacciotti, F., Hirth, G. A., & Natta, A. 1996, *A&A*, 310, 309
 Bacciotti, F., Mundt, R., Ray, T. P., Eislöffel, J., Solf, J., & Camenzind, M. 2000, *ApJ*, 537, 49
 Bertout, C., Robinchon, N., & Arenou, F. 1999, *A&A*, 352, 574
 Calvet, N. 1997, in *IAU Symp. 182, The Properties of T Tauri Winds*, ed. B. Reipurth & C. Bertout (New York: Springer), 417
 de Gouveia Dal Pino, E. M., & Benz, W. 1994, *ApJ*, 435, 261
 Dougados, C., Cabrit, S., Lavalley, C., & Ménard, F. 2000, *A&A*, 357, L61
 Dougados, C., Cabrit, S., & Lavalley-Fouquet, C. 2002, *Rev. Mexicana Astron. Astrofis. Conf. Ser.* 13, 43
 Eislöffel, J., & Mundt, R. 1998, *AJ*, 115, 1554
 Eislöffel, J., Mundt, R., Ray, T. P., & Rodríguez, L. F. 2000, *Protostars and Planets IV*, ed. V. Mannings, A. P. Boss, & S. S. Russell (Tucson: Univ. Arizona Press), 815
 Folha, D. F. M., & Emerson, J. P. 1999, *A&A*, 352, 517
 Garcia, P. J. V., Cabrit, S., Ferreira, J., & Binette, L. 2001, *A&A*, 377, 609
 Goodson, A. P., Böhm, K. H., & Winglee, R. M. 1999, *ApJ*, 524, 142
 Hartigan, P., Edwards, S., & Ghandour, L. 1995, *ApJ*, 452, 736
 Hartmann, L. 1998, *Accretion Processes in Star Formation* (Cambridge: Cambridge Univ. Press)
 Herbig, G. H., & Bell, K. R. 1988, *Lick Obs. Bull.*, 1111
 Hester, J. J., Stapelfeldt, K. R., & Scowen, P. A. 1998, *AJ*, 116, 372
 Hirth, G. A., Mundt, R., & Solf, J. 1997, *A&AS*, 126, 437
 Hirth, G. A., Mundt, R., Solf, J., & Ray, T. P. 1994, *ApJ*, 427, L99
 Kwan, J., & Tademaru, E. 1988, *ApJ*, 332, L41
 ———. 1995, *ApJ*, 454, 382
 Leinert, Ch., Zinnecker, H., Weitzel, N., Christou, J., Ridgway, S. T., Jameson, R., Haas, M., & Lenzen, R. 1993, *A&A*, 278, 129
 Mundt, R., & Eislöffel, J. 1998, *AJ*, 116, 860
 Mundt, R., Ray, T. P., & Raga, A. C. 1991, *A&A*, 252, 740
 Osterbrock, D. E. 1989, *Astrophysics of Gaseous Nebulae and Active Galactic Nuclei* (Mill Valley: University Science Books)
 Petrov, P. P., Gahm, G. F., Gameiro, J. F., Duemmler, R., Ilyin, I. V., Laakonen, T., Lago, M. T. V. T., & Tuominen, I. 2001, *A&A*, 369, 993
 Ray, T. P., Mundt, R., Dyson, J. E., Falle, S. A. E. G., & Raga, A. C. 1996, *ApJ*, 468, L103
 Reipurth, B., & Bally, J. 2001, *ARA&A*, 39, 403
 Reipurth, B., Heathcote, S., Yu, K., Bally, J., & Rodríguez, L. F. 2000, *ApJ*, 534, 317
 Shang, H., Glassgold, A. E., Shu, F. H., & Lizano, S. 2002, *ApJ*, 564, 853
 Solf, J. 1997, in *IAU Symp. 182, Spectroscopic Signatures of Microjets*, ed. B. Reipurth & C. Bertout (Dordrecht: Kluwer), 63
 Wichmann, R., Bastian, U., Krautter, J., Jankovics, I., & Ruciński, S. M. 1998, *MNRAS*, 301, L39